Phase Field Study of Discontinuous Precipitation in a Miscibility Gap System

J. Phase Equilib. Diffus. (2024) 45:1079–1087
https://doi.org/10.1007/s11669-024-01155-2

ORIGINAL RESEARCH ARTICLE

Phase Field Study of Discontinuous Precipitation in a Miscibility Gap System

Deepjyoti Mukherjee[1,2] · Henrik Larsson[2] · Joakim Odqvist[2]

Submitted: 28 February 2024 / in revised form: 7 August 2024 / Accepted: 11 September 2024 / Published online: 24 September 2024

Abstract A phase field model is developed to study the discontinuous (cellular) precipitation (DP) reaction in a hypothetical A-B miscibility gap system. Unlike previous treatments, the model employs an interaction energy term which couples the composition and the phase field variable to enable the necessary grain boundary movement. The influence of factors such as interaction energy, interfacial mobility and grain boundary diffusivity on the transformation rate and overall microstructure evolution are discussed.

Keywords DIGM · discontinuous precipitation · grain boundary diffusion · phase field modeling · phase transformation

1 Introduction

When studying precipitation in the binary Au-Ni system, Underwood[1] concluded that instead of nearly homogeneous nucleation of precipitates "The initial transformation product can be considered to be small hemispheres growing out from the grain boundary in three dimensions..." and "Transformation at low temperatures is characterized by a lamellar precipitate...". At the time, these were surprising results[2] since the experiments were conducted inside the miscibility gap, and the old concept of limit of metastability[3] (now called the spinodal) had been in the limelight for quite some time.[4] Later, Cahn concluded that due to the strong coherency stresses emerging from a large lattice misfit spinodal decomposition was suppressed in Au-Ni and the precipitation was instead clearly cellular.[5]

Cellular precipitation, or discontinuous precipitation (DP) in the classical sense, is a precipitation mechanism where a precipitate phase, together with a solute-depleted matrix, forms a lamellar product behind a migrating grain boundary.[6-9] When observed in miscibility gap systems both the solute-depleted matrix and the precipitate phase not only have the same crystal structure as the matrix phase but also the same crystal orientation as the adjoining grain.[10,11] The DP reaction has been observed in numerous binary, ternary and higher order systems,[12,13] and leads to both wanted[14,15] and unwanted[16,17] effects on mechanical properties.

The classical DP reaction has been treated theoretically by many authors.[18-30] The early models did not include any mechanism for migration of the grain boundary behind which the lamellar precipitate phase grows.[18-20] By considering different mechanisms that dissipate energy from the total available driving force for DP, Hillert[21] suggested, using Gibbs energy diagrams, that a deviation from local equilibrium is necessary for the DP reaction to occur. The friction force (solute drag) originating from dissipation of Gibbs energy due to diffusion inside the boundary will at high growth rates decrease, and at the same time the deviation from local equilibrium increases resulting in a

This invited article is part of a special tribute issue of the *Journal of Phase Equilibria and Diffusion* dedicated to the memory of Mats Hillert on the 100th anniversary of his birth. The issue was organized by Malin Selleby, John Ågren, and Greta Lindwall, KTH Royal Institute of Technology; Qing Chen, Thermo-Calc Software AB; Wei Xiong, University of Pittsburgh; and *JPED* Editor-in-Chief Ursula Kattner, National Institute of Standards and Technology (NIST).

✉ Joakim Odqvist
odqvist@kth.se

[1] Department of Industrial and Materials Science, Chalmers University of Technology, Gothenburg 41296, Sweden

[2] Department of Materials Science and Engineering, KTH Royal Institute of Technology, Stockholm 10044, Sweden

pulling force on the grain boundary during DP.[21] Later, when reviewing the available theories of DP, Hillert[22] showed that coherency strains in a thin film in front of the migrating grain boundary decreased the dissipation of Gibbs energy due to diffusion in the matrix phase and thus provided a driving force for the migration of the grain boundary during a DP reaction.

Since the DP reaction involves a complex interplay of many parameters and moving boundaries resulting in a characteristic morphology a natural choice when modelling this reaction is the phase-field method.[31] Only a few phase-field models of the DP reaction can be found in the literature, see e.g.,[6,28,29] and they treat exclusively the classical DP reaction. In (Ref 6,28) no physical mechanism is considered for the grain boundary movement. In (Ref 29) a finite interface dissipation model is used, but it is not clear what the mechanism for grain boundary movement is. In (Ref 32) the main objective was to study the effect of grain boundaries on the spinodal decomposition reaction in a binary system using a phase-field model. For some values of the atomic mobility at the grain boundary and grain boundary mobility the authors observed a lamellar structure behind a moving grain boundary, resembling discontinuous precipitation. They introduced a new concept, discontinuous spinodal decomposition, and developed a theory for it. Again, these authors did not consider any physics based mechanism for the grain boundary movement.

In the present work we develop a phase-field model of the DP reaction in a hypothetical miscibility gap system suitable for numerical simulations. In contrast to earlier treatments, our model includes a recently developed model for DIGM (Diffusion Induced Grain boundary Migration),[33] which is considered to be an important part of the DP reaction.[34] In the model for DIGM the grain boundary moves as a result of the coherency strain mechanism as discussed by Hillert,[22] and originally suggested by Sulonen.[35] Unlike[32] we name the reaction DP since it fulfills the requirements for this reaction i.e. a discontinuous change in both concentration and crystal orientation when crossing the reaction front. All simulations were performed using an in-house phase field code YAPFI,[36] which is based on the Wheeler-Boettinger-McFadden phase field model.[37]

The structure of this work is as follows. In Sect. 2 the employed phase-field model is described, followed by plain but detailed descriptions of the simulations carried out in Sect. 3. Simulation results are then discussed in some detail in Sect. 4 followed by conclusions in Sect. 5.

2 Phase Field Model for Discontinuous Precipitation

The microstructural evolution during DP is governed by two equations which take into account the variables that define the state of the system. In the present work, two kinds of variables are used: phase field variables for phase/grain identities and concentration variables. The evolution of phase-field variables ϕ_j are governed by the Allen-Cahn equation:[38]

$$\dot{\phi}_j = -M_\phi \frac{\delta G}{\delta \phi_j} \qquad \text{(Eq 1)}$$

where M_ϕ is a kinetic parameter related to the interfacial mobility. The ϕ_j denotes the phase-field variable for the *jth* grain. The evolution of the composition field is governed by the Cahn-Hilliard equation[39]:

$$\dot{c}_k = \nabla \cdot \left[M_k c_k \nabla \left(\frac{\delta G}{\delta c_k} \right) \right] \qquad \text{(Eq 2)}$$

where c_k and M_k are the concentration and mobility of component k, respectively. The formulation in Eq 2 is valid in a lattice-fixed frame of reference. However, in the present work the mobilities are the same for both components and a single constant molar volume is used and there is therefore no difference between the volume- and lattice-fixed frame of references.

Equations 1 and 2 yield the evolution of the microstructure. $\delta G/\delta \phi_j$ and $\delta G/\delta c_k$ are the functional derivatives of the Gibbs energy functional with respect to phase-field variable j and concentration variable k, respectively.

The Gibbs energy functional is given by

$$G = \int \left[g_0 - \sum \nabla c_k \cdot \sum \nabla c_i \kappa_{ki} - \sum \nabla \phi_j \cdot \sum \nabla \phi_m \varepsilon_{jm} \right] dV, \qquad \text{(Eq 3)}$$

where g_0 is Gibbs energy per unit volume, excluding gradient energy contributions, and κ_{ki} and ε_{jm} are gradient energy coefficients; since only two components and two grains are considered only one κ_{ki} and one ε_{jm} were used in simulations ($\kappa_{kk} = \varepsilon_{jj} = 0$). The sum of the phase-field variables is always equal to one, $\sum \phi_j = 1$

For convenience, g_0 is divided into two parts,

$$g_0 = g_1 + g_2. \qquad \text{(Eq 4)}$$

g_1 is a weighted average of the molar Gibbs energies of the phases. In the present work only a single phase α is present and g_1 is then simply given by

$$g_1 = G_m^\alpha / V_m \quad [\mathrm{J \cdot m^{-3}}] \qquad \text{(Eq 5)}$$

where G_m^{α} is the molar Gibbs energy of the α phase and V_m is the molar volume.

The term g_2 is a function of composition and state, i.e.,

$$g_2 = f(\boldsymbol{\phi}, \mathbf{c}) \quad \text{(Eq 6)}$$

The term g_2 is divided into two parts,

$$g_2 = g_{21} + g_{22} \quad \text{(Eq 7)}$$

where the former contains a contribution to the interfacial energy (a so-called double well potential) and the latter is an interaction term coupling phase-field variables and composition. The term g_{21} is given by,

$$g_{21} = W \sum \phi_j^2 \left(1 - \phi_j\right)^2, 0 \le \phi \le 1 \quad \text{(Eq 8)}$$

The term g_{22} holds an energetic coupling which is generated due to nucleation of DP at the interface. According to Hillert and Purdy[34] the grain boundary diffusivity plays a major role in the development of the initial driving force for the boundary motion. Due to the instability of the supersaturated phase and a higher grain boundary diffusivity, the nuclei are observed to form first at a grain boundary. This generates a strain energy due to the concentration gradient across the interface. Taking into consideration such energy change, the interaction term related to the elastic strain energy was, in line with the authors model for DIGM,[33] in the present work written as (considering that only two phase-field variables ϕ_1 and ϕ_2 and two components A and B were used),

$$g_{22} = K\phi_1(1 - \phi_1)\left(x_A - x_A^0\right)^2, 0 \le \phi \le 1 \quad \text{(Eq 9)}$$

where x_A is the local mole fraction of component A and $x_A^0 = 0.5$ is the average mole fraction of A. The K parameter was given by Hillert[40] as,

$$K = \frac{E\eta^2}{(1 - v)} \quad [\mathrm{J \cdot m^{-3}}] \quad \text{(Eq 10)}$$

where E is Young's modulus, η is the lattice misfit due to compositional variation and v is Poisson's ratio. The interaction term, given by Eq 9, generates a driving force only along the grain boundary. As discussed in,[33] when using Eq 9, the direction of motion is arbitrary in the beginning of the precipitation process. Some believe that the direction could be decided by the shape of the boundary while others say that it depends on the chemical forces.[41] Here, it was observed that the direction is random for a straight grain boundary but can be preferential if a curved boundary is used.

3 Simulations

As already mentioned, the DP reaction is controlled by many parameters and their interdependence. Therefore, in this section a parametric study for a binary system A-B inside a miscibility gap and with two grains separated by a grain boundary is described.

3.1 Base Simulation

As a baseline, a simulation was carried out using the following set-up and parameter values.

All simulations were carried out in 2D. The domain size was $(32 \cdot 10^{-9})^2\,[\mathrm{m^2}]$. Adaptive meshing was used and the resulting grid spacing was in the range $6.25 \cdot 10^{-11} - 2.5 \cdot 10^{-10}\,[\mathrm{m}]$. The adaptation of the grid was based on the local gradients in both composition and phase-field.

A planar grain boundary sectioned the domain into two rectilinear parts of equal size. Periodic boundary conditions were applied on the two sides of the domain orthogonal to the grain boundary. Closed boundary conditions were applied on the other two sides.

The initial composition field contained a uniformly distributed random noise $\Delta x_A = 0.01$ such as $x_A = x_A^0 \pm \Delta x_A$ at $t = 0$ where $x_A^0 = 0.5$.

The molar Gibbs energy was given by

$$G_m^{\alpha} = RT(x_A \ln x_A + x_B \ln x_B) + x_A x_B \cdot 30000 \quad [\mathrm{J \cdot mol^{-1}}] \quad \text{(Eq 11)}$$

i.e. a regular solution with a positive regular solution parameter $L = 30000$, which will induce a miscibility gap at the temperature used in simulations, 1000 K (isothermal). The equilibrium compositions at 1000 K are $x_A^{\alpha'} = 0.0333$ and $x_A^{\alpha''} = 0.9667$, respectively.

The κ_{AB} gradient energy parameter,

$$\kappa_{AB} = 3 \cdot 10^{-16} \cdot V_m \quad [\mathrm{J \cdot m^5 \cdot mol^{-2}}] \quad \text{(Eq 12)}$$

κ_{AB}/V_m is roughly proportional to the square of a typical metallic system lattice parameter times the regular solution parameter[39].

The prefactor W and the gradient energy ε_{12} were set to yield an interfacial width of approximately 0.5 nm and an interfacial energy of approximately $0.1\,\mathrm{J/m^2}$,[42] viz.

$$W = 12000/V_m \quad [\mathrm{J \cdot m^{-3}}] \quad \text{(Eq 13)}$$

$$\varepsilon_{12} = 1.875 \cdot 10^{-16}/V_m\,[\mathrm{J \cdot m^{-1}}] \quad \text{(Eq 14)}$$

The interaction parameter K was set to

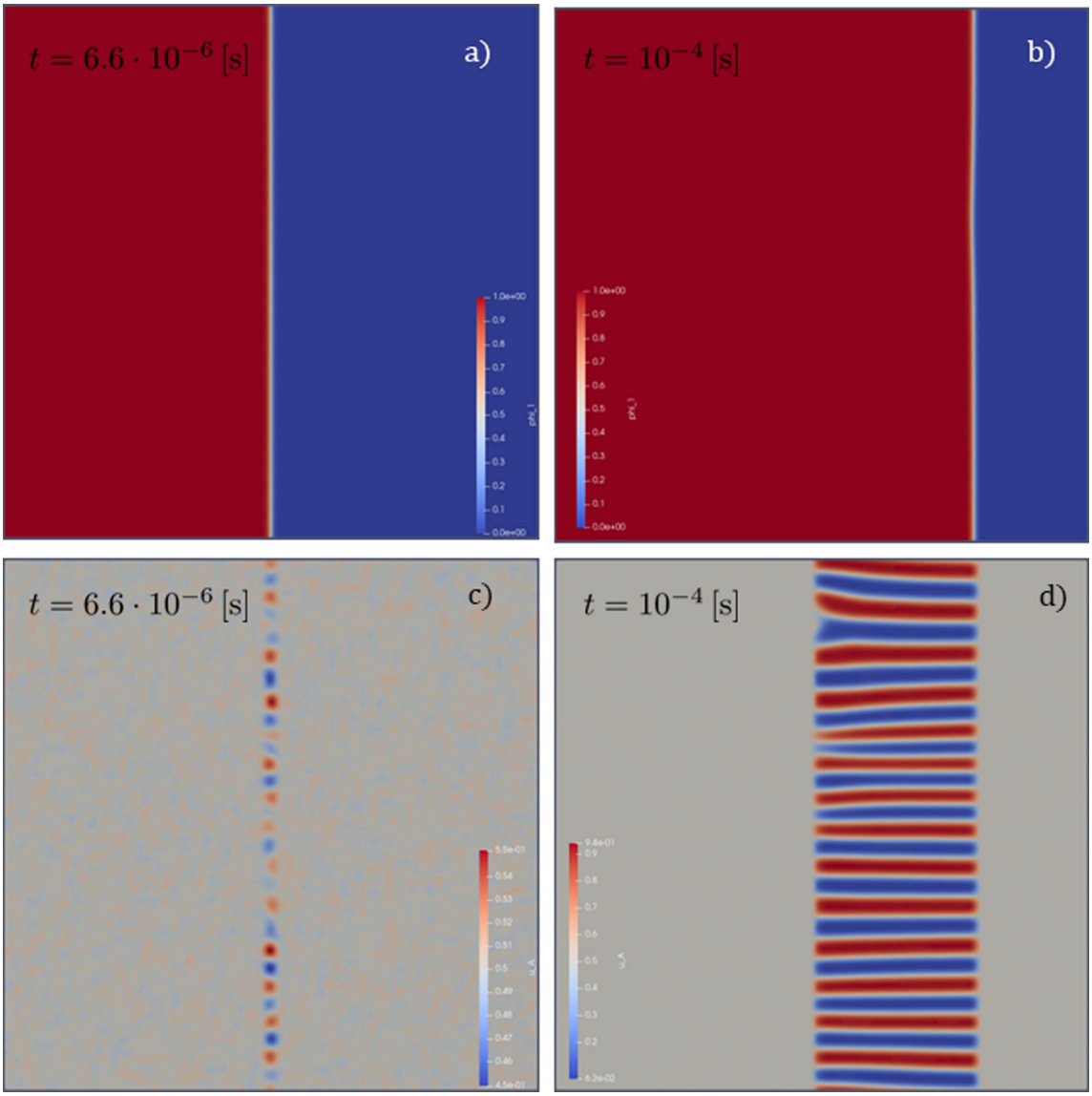

Fig. 1 Results from simulation of discontinuous precipitation using the baseline set-up. (a/b) and (c/d) show ϕ_1 and mole fraction A, x_A, respectively. (a) and (c) show results after a very short time, $6.6 \cdot 10^{-6}$ s, and b) and d) after 10^{-4} s. For (c), the scale runs from $x_A = 0.45$ to $x_A = 0.55$, whereas for d) it runs from $x_A = 0.062$ to $x_A = 0.94$

$$K = 1000/V_m \quad [\mathrm{J} \cdot \mathrm{m}^{-3}] \tag{Eq 15}$$

The mobilities and phase-field mobility were set to the following values

$$M_A^\alpha = M_B^\alpha = 10^{-21} \quad [\mathrm{mol} \cdot \mathrm{m}^2 \cdot \mathrm{J}^{-1} \cdot \mathrm{s}^{-1}] \tag{Eq 16}$$

$$M_\phi = 10^6 \cdot V_m \quad [\mathrm{m}^3 \cdot \mathrm{s}^{-1} \cdot \mathrm{J}^{-1}] \tag{Eq 17}$$

In order to take grain boundary diffusion into account, the component mobilities were modified as follows

$$M_k^{\alpha tot} = M_k^\alpha \left[1 + F_{gb} \sum \phi_j (1 - \phi_j)\right] \tag{Eq 18}$$

and it can be seen that the modification is only active at the grain boundary. A factor $F_{gb} = 10^5$ was used.

The molar volume was arbitrarily set to $V_m = 10^{-5}\,[\mathrm{m}^3 \cdot \mathrm{mol}^{-1}]$, but this value does not affect simulations.

Results from the base simulation are shown in Fig. 1.

3.2 Variations of the Base Simulation

The effect of grain boundary mobility (compared to the mobility in the bulk), interaction parameter, phase-field mobility, shape of the grain boundary and gradient energy coefficient was studied, one parameter at the time. Only those simulation settings explicitly stated differ from the settings of the base simulation.

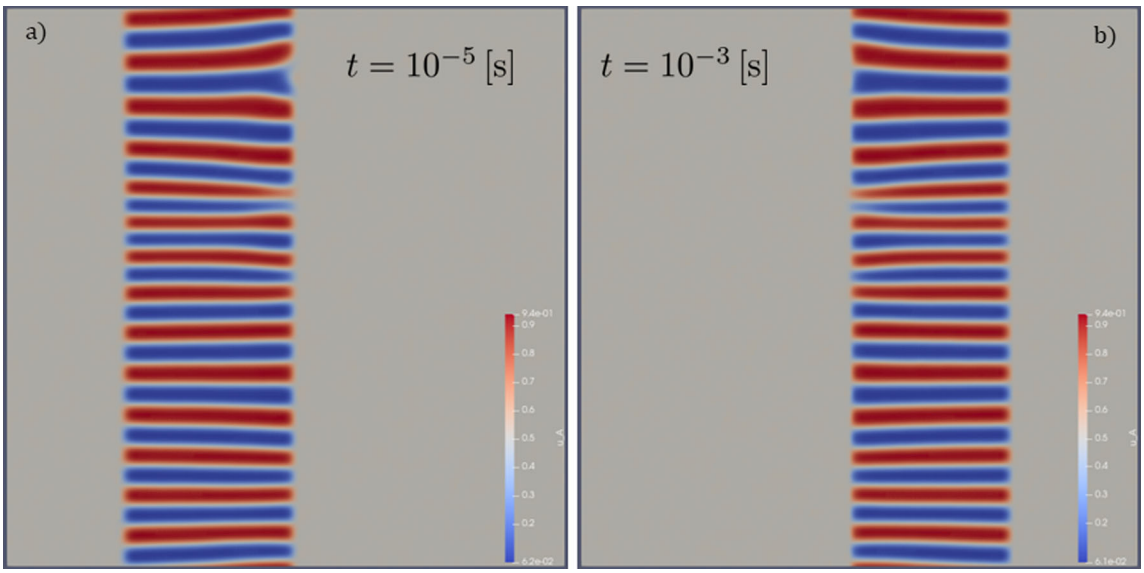

Fig. 2 Results from simulation of discontinuous precipitation where the factor F_{gb} was varied compared to the baseline set-up. (a) show results from a simulation where $F_{gb} = 10^4$ after $t = 10^{-5}$ [s] and (b) where $F_{gb} = 10^6$ after $t = 10^{-3}$ [s]

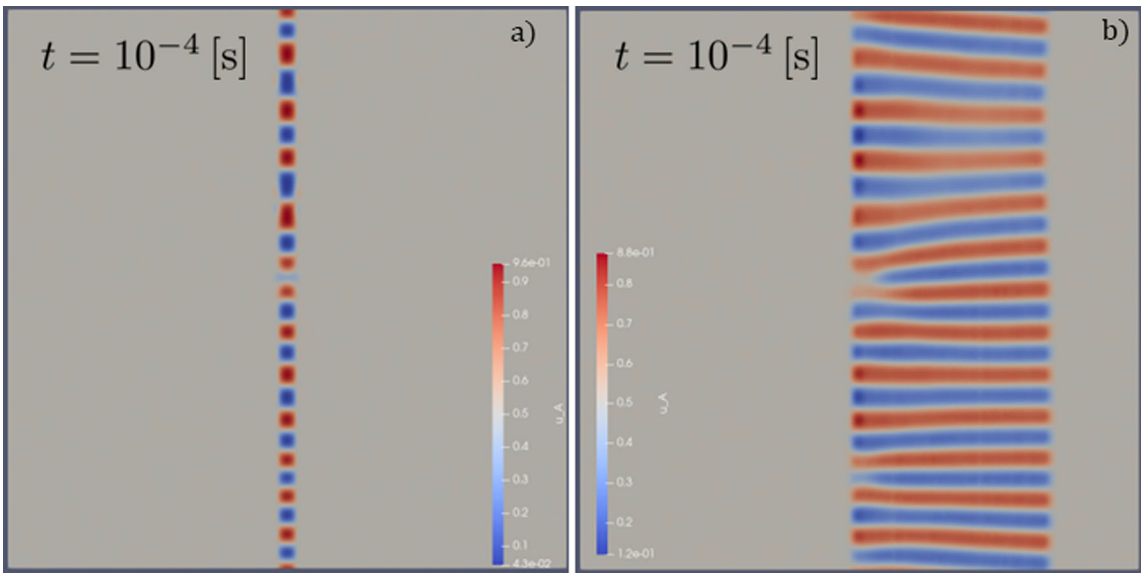

Fig. 3 Results from simulation of discontinuous precipitation at $t = 10^{-4}$ [s] where the interaction parameter K was varied compared to the baseline set-up. (a) show results from a simulation where $K \cdot V_m = 10^2$ and (b) where $K \cdot V_m = 10^4$. For (a) the scale is in the range $0.043 \leq x_A \leq 0.96$ and for (b) $0.12 \leq x_A \leq 0.88$

3.2.1 *Variations of the Ratio of Bulk to Grain Boundary Mobility*

Simulations were performed with $F_{gb} = 10^4$ and $F_{gb} = 10^6$ (see Eq 18), i.e. an order of magnitude above and below that of the base simulation. Results from these simulations are shown in Fig. 2.

3.2.2 *Variations in Magnitude of Interaction Parameter K*

Simulations were performed with $K \cdot V_m$ equal to 10^2 and 10^4, see Fig. 3.

3.2.3 *Variations in M_ϕ*

Simulations were performed with M_ϕ / V_m equal to 10^4 and 10^8, see Fig. 4.

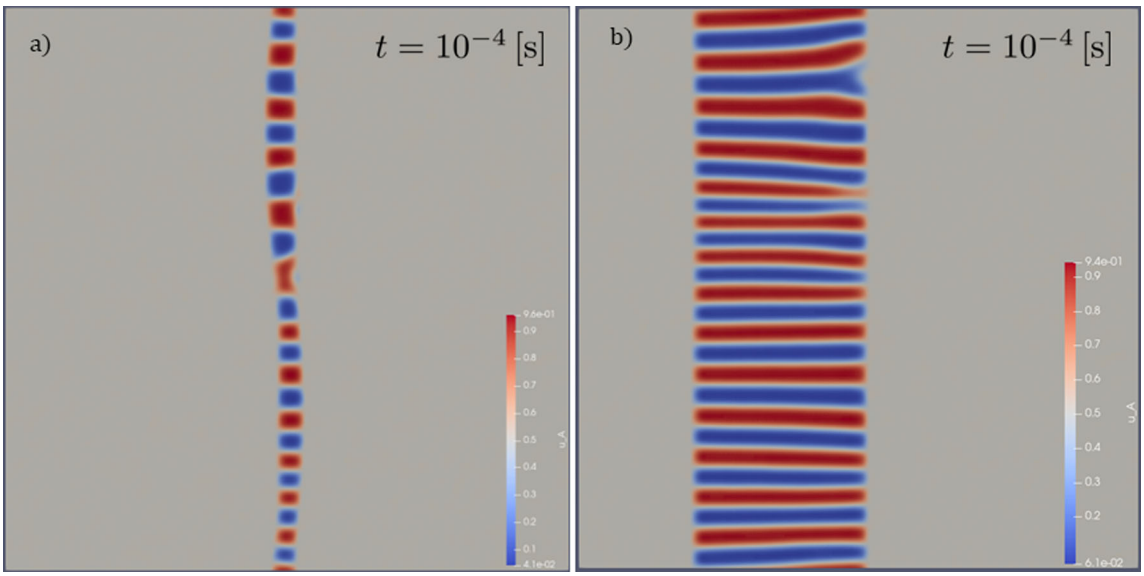

Fig. 4 Results from simulation of discontinuous precipitation at $t = 10^{-4}$ [s] where M_ϕ was varied compared to the baseline set-up. (a) show results from a simulation where $M_\phi/V_m = 10^4$ and (b) where $M_\phi/V_m = 10^8$

3.2.4 An Initially Sinusoidal Grain Boundary

As opposed to the initially planar grain boundary of the base simulation, a set-up was also used where the grain boundary has an initial sinusoidal shape, see Fig. 5.

3.2.5 Variations in Gradient Energy Coefficient κ_{AB}

Finally, simulations were performed with κ_{AB} set to a third and three times higher, respectively, compared to the baseline set-up, see Fig. 6. For these simulations the initially sinusoidal grain boundary was used.

4 Results and Discussion

The simulations in Sect. 3 mimic a heat treatment of the hypothetical single phase alloy A-B (50 % A and 50 % B), at a temperature well inside the symmetric miscibility gap. At time $t = 0$ random concentration fluctuations around the average composition are applied in the whole simulation domain. In all simulations the phase-field variable, ϕ, varies from zero (blue) to one (red), see Fig. 1(a) and (b), and Fig. 5(a). The red and blue domains in those ϕ plots correspond to two grains joined by a thin grain boundary, where $0 < \phi < 1$. Although the random concentration fluctuations are applied in the whole simulation domain spinodal decomposition is effectively suppressed everywhere except inside the grain boundary, see Fig. 1(c). This is due to the very low atomic mobilities set in the grains compared to the grain boundary. The suppressed decomposition is very faintly discernible as a substructure in the two grains while precipitation of alternating A-rich (red) and B-rich (blue) lamellae starts at the grain boundary where the atomic mobilities are much higher, see Fig. 1(c). It should be emphasized that the model is not prescribing any direction of growth; it is random for the planar boundary. In Fig. 1 it moves to the right, and in Fig. 2(a) to the left or to the right in Fig. 2(b). This is an effect of the interaction term used, Eq 9, as discussed in.[33] For the sinusoidal grain boundary, see e.g. Fig. 5, the direction of growth is however also affected by the boundary curvature.

Once the decomposition along the grain boundary has reached a certain degree the lamellae grow at an essentially constant velocity, though the velocity is given by a complex interplay between the different parameters. These predictions are qualitatively in agreement with experimental findings reported by Ma et al.[10] for the system TiC-ZrC. The carbide system TiC-ZrC has interesting properties for e.g. as a second hard phase in cemented carbide tools. It shows a wide miscibility gap with a critical temperature as high as 2200 $^\circ C$. The alternating Ti-rich and Zr-rich TiZrC lamella nucleating at and growing from essentially straight grain boundaries can be seen in Fig. 5(b) in.[10] In addition, as can be seen from EBSD images in their Fig. 9 (a) and (b), the lamellae growing behind the moving grain boundary inherit the crystal orientation of the adjoining grain. This is also what our simulation predicts, see Fig. 1(b) and (d).

A prerequisite for growth to occur at all is that the interaction parameter K in Eq 10 has a sufficient magnitude. Given that K is large enough for growth to occur, the growth velocity increases monotonically, but asymptotically, with increasing K (see Fig. 3); there will be an

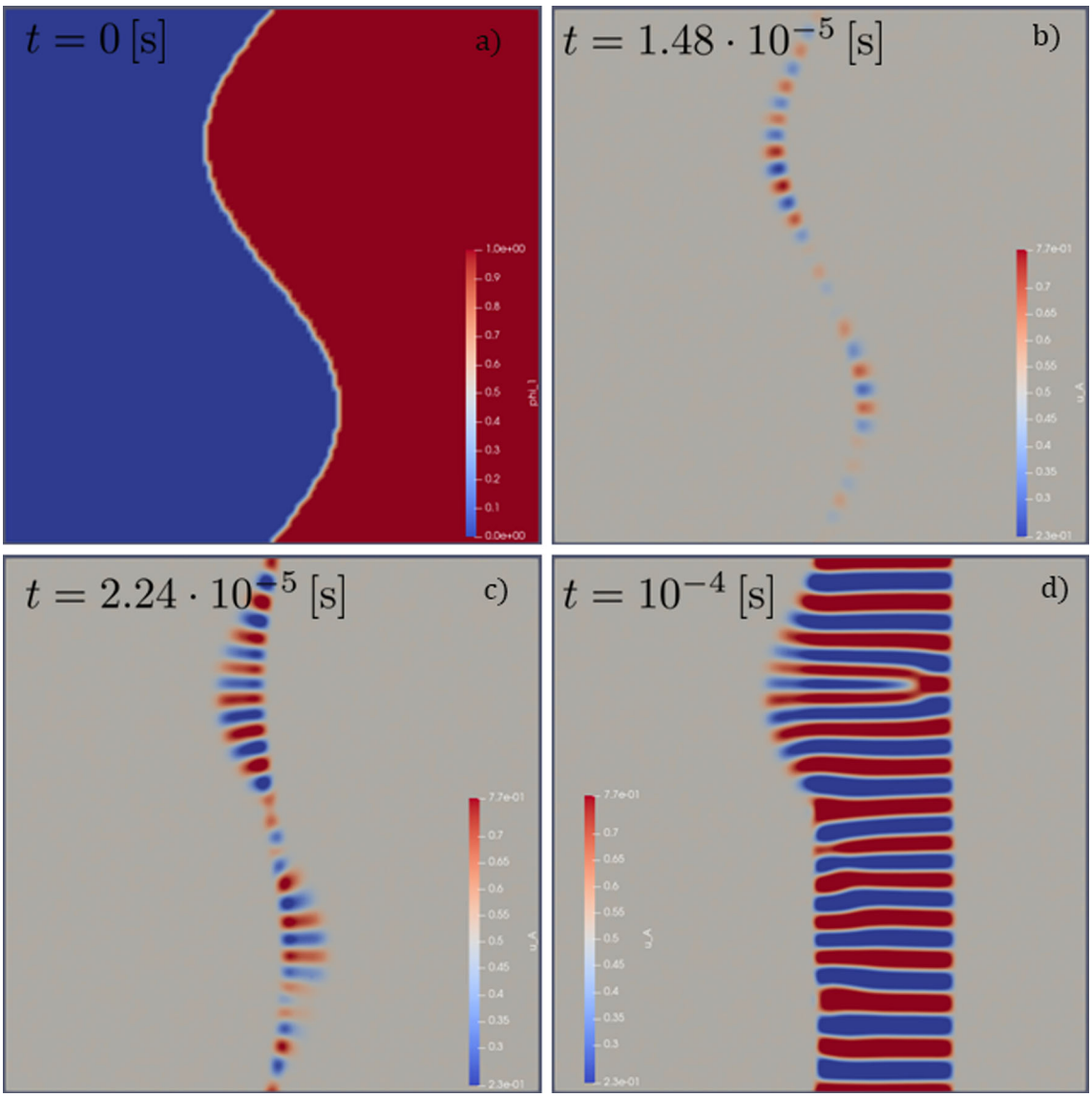

Fig. 5 Results from simulation of discontinuous precipitation with an initially sinusoidal grain boundary. (a) show the phase field at $t = 0$, and (b)-(d) show the evolution of the composition field

asymptotic behavior due to the factor $(x_A - x_A^0)^2$ in Eq 9; some diffusion is necessary. To trigger the growth, it is also necessary that the growth direction is determined by a random perturbation or by the influence of curvature. It should be emphasized that the parameter K is missing from all previous phase-field treatments of DP. Instead, a sufficiently high phase-field mobility M_ϕ was chosen. M_ϕ will not affect the reaction rate if it is high enough. Comparing Fig. 1(d) and 4(b) it can be seen that the results are virtually identical with $M_\phi/V_m = 10^6$ and $M_\phi/V_m = 10^8$, but with $M_\phi/V_m = 10^4$ the phase-field mobility has become rate determining.

With sufficiently high K and M_ϕ the rate determining process is the diffusion along the grain boundary, emphasizing the importance of the relation of atomic mobility in the grain boundary and in the bulk of the grains, also highlighted in a previous model of DP.[6] This is illustrated by comparing Fig. 1 and 2, where the only varying parameter is F_{gb}. In such a regime and with the lamellae thickness remaining essentially constant the growth rate will also be essentially constant since the diffusion distance and the driving force is in steady state at the growth front.

The gradient energy coefficient κ_{AB} determines the critical wavelength of the spinodal decomposition and thus determines the size of the lamellae embryos during the early stages of the process, which is then carried over to the growth regime as can be seen in Fig. 6. With the rate determining process being the lateral diffusion between A-

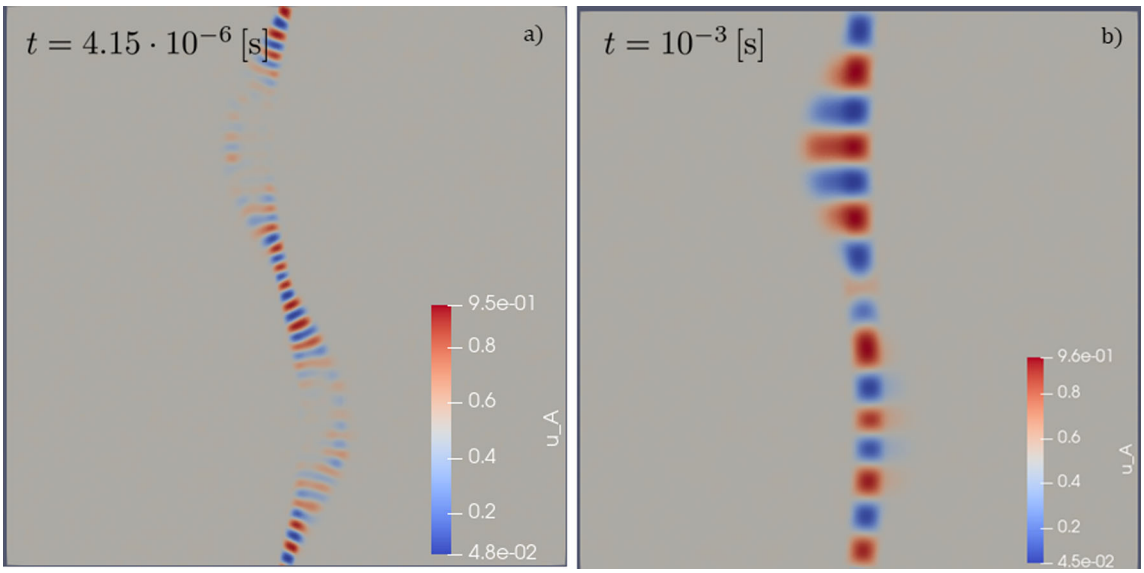

Fig. 6 Results from simulations of discontinuous precipitation with a lower $\kappa_{AB} = 1 \cdot 10^{-16} \cdot V_m$ (a)) and a higher $\kappa_{AB} = 9 \cdot 10^{-16} \cdot V_m$ (b) compared to the baseline set-up

and B-rich lamellae this will affect the growth rate; for the range of κ_{AB} values studied in the present work the growth will be faster the thinner the lamellae. This is in line with the observations made in.[32] Since thinner lamellae also mean a larger amount of gradient energy per unit volume there will presumably exist some lower limit on the thickness below which the growth rate will decrease. When performing simulations with varying κ_{AB} and a planar boundary it was observed for the largest value that the local variation in conditions was insufficient to trigger the growth; this will happen with wider lamellae embryos and the same initial composition fluctuations. This is the reason why a sinusoidal grain boundary was used for the simulations when varying κ_{AB}, see Fig. 6.

5 Conclusions

A phase field model for DP in a miscibility gap system has been developed. The simulations reproduced several experimentally observed features. The influence of grain boundary diffusion (F_{gb}), gradient energy coefficient (κ_{AB}), interface mobility (M_ϕ), interaction parameter (K) and grain boundary curvature on the microstructural evolution was studied. Some conclusions can now be drawn:

- For a model to capture the effects of different initial shapes of the grain boundary on the microstructure evolution during DP, reported in experimental studies, curvature driven boundary migration is not sufficient. There is a need for an additional driving force. In our case this driving force comes from the coherency strain energy mechanism suggested by Sulonen.[35]
- As in previous models, the magnitude of the atomic mobility in the grain boundary in relation to the mobility in the bulk of the grains is crucial.

In addition, the DP reaction in miscibility gap systems was discovered, see e.g. [1], for systems where Cahn's theory of coherent spinodals[5] was thought to be operating, but instead of a spinodal decomposition mechanism at lower temperatures DP was found.[2] This raises the question if an adequate difference in atomic mobilities is sufficient to get a quantitative correspondence between simulations and experiments of the DP reaction in miscibility gap systems, or if the model needs to handle the coherency strain contribution in the whole domain and not only in a thin zone close to the moving grain boundary. This question we will address in a separate paper for the system TiC-ZrC.

Acknowledgments We thank the Swedish Foundation for Strategic Research (RMA-15-0062), the Foundation for Applied Thermodynamics and the Swedish iron and steel producers' association for funding this research.

Funding Open access funding provided by Royal Institute of Technology.

References

1. E.E. Underwood, Precipitation in gold-nickel alloys. PhD thesis, Massachusetts Institute of Technology, Cambridge, MA, 1954.
2. J.W. Cahn, Reflections on Diffuse Interfaces and Spinodal Decomposition, in *The Selected Works of John W. Cahn* W.C. Carter and W.C. Johnson (Eds) TMS, pp. 1–8, 1998.
3. J.W. Gibbs, On the Equilibrium of Heterogeneous Substances, *Am. J. Sci.*, 1878, **3–16**(96), p 441–458.
4. G. Borelius, F. Larris, and E. Ohlsson, Kinetics of Precipitation in Pb-Sn Alloys, *Ark. Mat. Astron. Fys.*, 1944, **A31**, p 1–19.
5. J.W. Cahn, On Spinodal Decomposition, *Acta Metall.*, 1961, **9**, p 795–801.
6. L. Amirouche and M. Plapp, Phase-Field Modeling of the Discontinuous Precipitation Reaction, *Acta Mater.*, 2009, **57**(1), p 237–247.
7. C.S. Smith, Microstructure, *Trans. ASM*, 1953, **45**, p 533–575.
8. A.H. Geisler, Precipitation from solid solutions of metals, *Phase Transformations in Solids*. R. Smoluchowski, J. Mayer, W. Weyl Ed., Wiley, New York, 1951
9. E. Hornbogen, Systematics of the Cellular Precipitation Reactions, *Metall. Trans.*, 1972, **3**, p 2717–2727.
10. T. Ma, R. Borrajo-Pelaez, P. Hedström, I. Borgh, A. Blomqvist, S. Norgren, and J. Odqvist, Microstructure Evolution During Phase Separation in Ti-Zr-C, *Int. J. Refract Metal Hard Mater.*, 2016, **61**, p 238–248.
11. R.P. Babu, T. Ma, P. Hedström, and J. Odqvist, A Transmission Electron Microscopy Study of Discontinuous Precipitation in the High Misfit System (Ti, Zr)C, *Mater. Today Commun.*, 2020, **25**, p 101281.
12. P. Zieba, Recent Developments on Discontinuous Precipitation, *Arch. Metall. Mater.*, 2017, **62**(2), p 955–968.
13. D.B. Williams and E.P. Butler, Grain Boundary Discontinuous Precipitation Reactions, *Int. Mater. Rev.*, 2012, **26**(1), p 153–183.
14. T. Ma, P. Hedström, V. Ström, A. Masood, I. Borgh, A. Blomqvist, and J. Odqvist, Self-Organizing Nanostructured Lamellar (Ti, Zr)C—A Superhard Mixed Carbide, *Int. J. Refract Metal Hard Mater.*, 2015, **51**, p 25–28.
15. Y. Li, H. Katsui and T. Goto, Effect of Heat Treatment on the Decomposition of TiC–ZrC Solid Solutions by Spark Plasma Sintering, *J. Eur. Ceram. Soc.*, 2016, **36**(15), p 3795–3800.
16. B. Hassan and J. Corney, Grain Boundary Precipitation in Inconel 718 and ATI 718Plus, *Mater. Sci. Technol.*, 2017, **33**(16), p 1879–1889.
17. H.F. Merrick, H.W. Hayden, and R.C. Gibson, Effect of Carbon and Titanium on the Hot Workability of 25Cr-6Ni Stainless Steels, *Metall. Trans.*, 1973, **4**(3), p 827–832.
18. D. Turnbull, Theory of Cellular Precipitation, *Acta Metall.*, 1955, **3**, p 55–63.
19. J.W. Cahn, The Kinetics of Cellular Segregation Reactions, *Acta Metall.*, 1959, **7**, p 18–28.
20. H.I. Aaronson and Y.C. Liu, On the Turnbull and the Cahn Theories of the Cellular Reaction, *Scr. Metall.*, 1968, **2**(1), p 1–7.
21. M. Hillert, The Role of Interfaces in Phase Transformations, *Mech. Phase Transform. Crystal. Solids*, 1969, **33**, p 231–247.
22. M. Hillert, On Theories of Growth During Discontinuous Precipitation, *Metall. Trans.*, 1972, **3**(11), p 2729–2741.
23. B.E. Sundquist, Cellular Precipitation, *Metall. Mater. Trans. B*, 1973, **4**(8), p 1919–1934.
24. M. Hillert, An Improved Model for Discontinuous Precipitation, *Acta Metall.*, 1982, **30**, p 1689–1696.
25. L.M. Klinger, Y.J.M. Brechet, and G.R. Purdy, On Velocity and Spacing Selection in Discontinuous Precipitation-I. SIMPLIFIED Analytical Approach, *Acta Metall.*, 1997, **45**(12), p 5005–5013.
26. E.A. Brener and D.E. Temkin, Theory of Diffusional Growth in Cellular Precipitation, *Acta Metall.*, 1999, **47**(14), p 3759–3765.
27. E.A. Brener and D.E. Temkin, Theory of Discontinuous Precipitation: Importance of the Elastic Strain, *Acta Mater.*, 2003, **51**(3), p 797–803.
28. L. Amirouche and M. Plapp, On the Effect of Bulk Diffusion on the Initiation of the Discontinuous Precipitation Reaction: Phase-Field Simulation, *Solid State Phenom.*, 2011, **172–174**, p 549–554.
29. T.C. Duong, R.E. Hackenberg, V. Attari, A. Landa, P.E. Turchi, and R. Arróyave, Investigation of the Discontinuous Precipitation of U-Nb Alloys via Thermodynamic Analysis and Phase-Field Modeling, *Comput. Mater. Sci.*, 2020, **175**, p 1–12.
30. O. Penrose and J.W. Cahn, On the Mathematical Modelling of Cellular (Discontinuous) Precipitation, *Discrete Contin. Dynam. Systems*, 2017, **37**, p 963–982.
31. N. Moelans, B. Blanpain, and P. Wollants, An Introduction to Phase-Field Modeling of Microstructure Evolution, *Calphad: Comput. Coupl. Phase Diagr. Thermochem.*, 2002, **32**(2), p 268–294.
32. H. Ramanarayan and T.A. Abinandanan, Grain Boundary Effects on Spinodal Decomposition II. Discontinuous Microstructures, *Acta Mater.*, 2004, **52**, p 921–930.
33. D. Mukherjee, H. Larsson, and J. Odqvist, Phase Field Modelling of Diffusion Induced Grain Boundary Migration in Binary Alloys, *Comput. Mater. Sci.*, 2020, **184**, p 1–9.
34. M. Hillert and G.R. Purdy, Chemically Induced Grain Boundary Migration, *Acta Metall.*, 1977, **26**, p 333–340.
35. M. Sulonen, On the Driving Force of Discontinuous Precipitation and Dissolution, *Acta Metall.*, 1964, **12**(9), p 749–753.
36. H. Larsson, The YAPFI Phase-Field Implementation, pp. 1–22, 2021.
37. A.A. Wheeler, W.J. Boettinger, and G.B. McFadden, Phase-Field Model for Isothermal Phase Transitions in Binary Alloys, *Phys. Rev. A*, 1992, **45**(10), p 7424–7440.
38. A.M. Samuel and J.W. Cahn, A Microscopic Theroy for Antiphase Boundary Motion and its Application to Antiphase Domain Coarsening, *Acta Metall.*, 1978, **27**, p 1085–1095.
39. J.W. Cahn and J.E. Hilliard, Free Energy of a Nonuniform System. I. Interfacial Free Energy, *J. Chem. Phys.*, 1958, **28**, p 258–267.
40. M. Hillert, On The Driving Force for Diffusion Induced Grain Boundary Migration, *Scripta Metall. Mater.*, 1983, **17**(1), p 237–240.
41. D. Duly and Y. Brechet, Nucleation Mechanism of Discontinuous Precipitation in MgAl Alloys and Relation with the Morphology, *Acta Metall. Mater.*, 1994, **42**(9), p 3035–3043.
42. J.A. Warren and W.J. Boettinger, Prediction of Dendritic Growth and Microsegregation Patterns in a Binary Alloy Using the Phase-Field Method, *Acta Metall. Mater.*, 1995, **43**, p 689–703.